Cerebral Cortex February 2006;16:254-267
doi:10.1093/cercor/bhi105
Advance Access publication May 11, 2005

The Human Parietal Operculum. I. Cytoarchitectonic Mapping of Subdivisions

Simon B. Eickhoff[1,2], Axel Schleicher[2], Karl Zilles[1,2] and Katrin Amunts[1,3]

[1]Institute of Medicine, Research Center Jülich, 52425 Jülich, Germany, [2]C. & O. Vogt-Institute for Brain Research, University of Düsseldorf, 40001 Düsseldorf, Germany and [3]Department of Pyschiatry and Psychotherapy, RWTH Aachen University, 52074 Aachen, Germany

The human secondary somatosensory cortex (SII) is located on the parietal operculum, as shown by intraoperative stimulation and functional imaging studies. The position and extent of the anatomical correlates of this functionally defined region, however, are still unknown. We have therefore histologically mapped the putative anatomical correlates of the SII cortex in cell-body-stained histological sections of 10 human postmortem brains using quantitative cytoarchitectonic analysis. The gray level index (GLI), which is an indicator of the volume fraction of nerve cell bodies, was measured in the parietal operculum. GLI profiles as measures of the laminar pattern of the cortex were extracted perpendicular to cortical layers. Cytoarchitectonic borders were detected observer-independently by multivariate statistical analysis of the laminar profiles. Four cytoarchitectonic areas (termed OP 1–4) were identified. This cytoarchitectonic heterogeneity of the parietal operculum corresponds to results of functional imaging studies on the human SII cortex and data from non-human primates where multiple subregions within SII have been demonstrated by electrophysiological and connectivity studies.

Keywords: brain mapping, cytoarchitecture, human cerebral cortex, SII, somatosensory cortex

Introduction

The concept of a secondary somatosensory cortex (SII) was introduced for the first time to describe a second cortical representation of the cat's feet next to the previously defined 'first' somatosensory area (Adrian, 1940). Homologous regions were also found in other mammals, including non-human primates (Burton, 1986). The first evidence for a human SII homologue was based on somatosensory sensations following electrical stimulation during neurosurgery in the region of the Sylvian fissure (Penfield and Jasper, 1954). Woolsey *et al.* (1979) confirmed these results using electrical stimulation and evoked potentials. In functional imaging studies, activations of SII have been reported for many experimental conditions, such as light touch (Ledberg *et al.*, 1995; Disbrow *et al.*, 2000), pain perception (Coghill *et al.*, 1994; Peyron *et al.*, 1999), visceral sensations (Lotze *et al.*, 2001; Aziz *et al.*, 2000) and tactile attention (Burton and Sinclair, 2000; Lam *et al.*, 2001). These activations, however, were distributed widely over the parietal operculum, ranging from a region at the level of the anterior commisure (Peyron *et al.*, 1999) to the retroinsular region (Xu *et al.*, 1997).

Evidence has been provided that the SII region of the macaque monkey can be subdivided into at least two parts (Fig. 1). Both subareas contain a separate complete body representation and can be distinguished from each other by their architecture and connectivity (Burton *et al.*, 1995; Krubitzer *et al.*, 1995). An analogous subdivision of the human SII cortex was subsequently proposed by Disbrow *et al.* (2000) based on functional magnetic resonance imaging (fMRI) data.

The microstructural anatomical correlates of the human SII region, however, have not yet been identified. The classical brain maps of Brodmann (1909), Vogt and Vogt (1919) and von Economo and Koskinas (1925), for example, differ greatly between each other in their nomenclature as well as in the number and location of candidate areas (Fig. 2, cf. Zilles, 2004). Brodmann's areas 40 and 43 both extend onto the parietal operculum and are therefore by their topography candidates for SII (Fig. 2). The opercular part of von Economo's and Koskinas' (1925) inferior parietal area P*F* (termed P*F*op) corresponds to parts of BA 40. The location of their subcentral area P*F*D corresponds roughly to the location of Brodmann's area (BA) 43. Thus P*F*op and P*F*D may be anatomical substrates for SII in the map of von Economo and Koskinas. On the basis of their myeloarchitectonic studies, Vogt and Vogt (1919) defined a subcentral area 72. In contrast to BA 43 or P*F*D, this area barely reaches the anterior part of the subcentral cortex rostral to the central sulcus. Their area 88 (located on the inferior supramarginal gyrus) may correspond to parts of area P*F*op. Additionally, Vogt and Vogt (1919) defined two areas in the depth of the Sylvian fissure, areas 73 (rostrally) and 74 (caudally), which have no homologues in the maps of Brodmann (1909) and von Economo and Koskinas (1925). It must be emphasized that the classical architectonic maps relied purely on visual inspection of histological sections. The criteria for the definition of cytoarchitectonic borders thus depended considerably on the observers experience. Differences between the criteria used by the authors and the biological variability between the examined brains, in particular given the small sample sizes of these classical brain mapping studies, presumably influenced the results of former architectonic approaches. This may have led to the differences in the available maps above described. In addition, all these maps represent schematic two-dimensional drawings without information about stereotaxic location and intersubject variability. They also rarely provide information about the cortical areas within the sulci, but show schematic projections onto the cortical surface. The larger portion of cortical areas is thus not shown, since the proportion of cortical surface hidden in sulci reaches two-thirds of the total surface (Zilles *et al.*, 1988). The functionally defined human SII region is hidden almost entirely in the Sylvian fissure, which makes its interpretation with respect to the classical maps almost impossible.

The aim of the present study was therefore, to analyze the cytoarchitecture of the parietal operculum (i.e. the region of SII) in serial histological sections of 10 human post-mortem brains

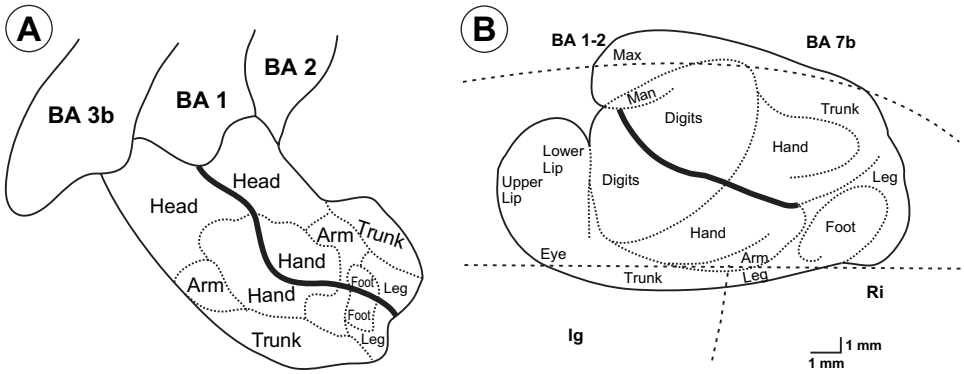

Figure 1. The macaque SII region based on electrophysiological recording (*A*, Krubitzer *et al.*, 1995) and connectivity of SI towards the Sylvian fissure (*B*, Burton *et al.*, 1995). Both authors suggest two distinct areas within the SII cortex. These areas contain mirror-like body representations, which are orientated from anterior–superficial (head) to posterior–deep (feet) and share a common border at the head–hand–feet line (bold line).

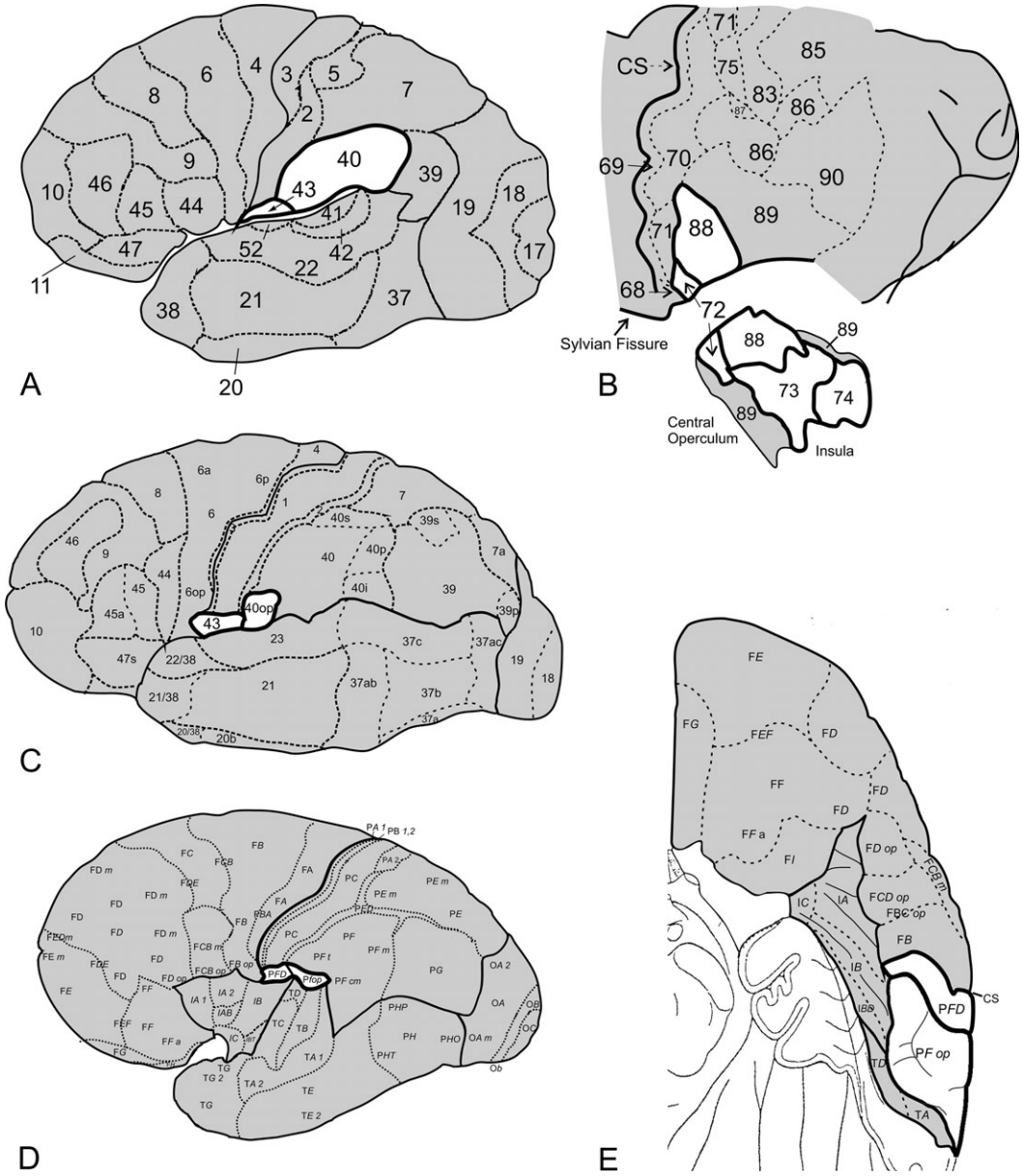

Figure 2. Architectonical brain maps adapted from (*A*) Brodmann (1909), (*B*) Vogt and Vogt (1919) and (*C*) Sarkissov (1949). The free parietal surface in a lateral (*D*) and the parietal operculum in a ventral view (E) in the map of Von Economo and Koskinas (1925). A bold line marks the regions containing the presumed SII cortex.

using a quantitative statistically testable approach for the observer-independent detection of borders between cortical areas (Schleicher *et al.*, 2000). The results of this mapping study will then be described in standard stereotaxic space and compared with the location of the human SII cortex as described in functional imaging (Eickhoff *et al.*, 2005).

Material and Methods

Ten post-mortem human brains (five male; Table 1) were obtained from the body donor program of the Anatomical Institute of the University of Düsseldorf. Subjects had no clinical history of neurological or psychiatric diseases. Handedness of the subjects was unknown. Considering a general incidence of 90% for right-handedness (Annett, 1973), it can be assumed that most cases were right handed. The brains were removed from the skull <24 h *post mortem* and fixed for ~6 months. The whole brains were embedded in paraffin and serially sectioned in a coronal plane (thickness = 20 μm). Each 15th section was stained for cell-bodies using a silver staining method (Merker, 1983). This method yields a higher contrast between black cell bodies and unstained neuropil as compared with traditional Nissl-staining. This contrast is an important prerequisite for automated cytoarchitectonic analysis. Every 4th stained section, i.e. every 60th of the whole series, was analyzed, resulting in a distance of 1.2 mm between examined sections.

Observer Independent Detection of Cortical Borders

Cortical borders were identified using the approach of Schleicher *et al.* (2000). In short, rectangular regions of interest (ROIs) were defined in both hemispheres of the histological sections (Fig. 3*B*). The ROIs were digitized in a meander-like sequence using a microscope with a motor stage for automated scanning and focusing (Fig. 3*C*). Images were processed using the KS 400 image analyzing software (Version 3.0, Zeiss/Germany). The gray level index (GLI; Schleicher and Zilles, 1990), estimating the volume fraction of cell bodies (Wree *et al.*, 1982), was measured by adaptive thresholding in continuously adjoining square measuring fields (32 × 32 μm). The resulting GLI image represents in each pixel the local volume fraction of cell bodies in the corresponding measuring field (Fig. 3*D*). Equidistant intensity profiles (thickness = 125 μm, spacing = 200 μm; Fig. 3*E*), which quantify the laminar GLI changes from the border between layers I and II to the border between layer VI and the white matter, were automatically obtained from the GLI images perpendicular to the cortical layers using a minimum length algorithm. Profiles were length normalized in order to compensate for local and individual variations in absolute cortical thickness. The shape of each profile was quantified by a vector of 10 features based on central moments (mean GLI, mean x, SD, skewness and kurtosis, as well as the analogous parameters from the absolute values of its first derivative) (Amunts *et al.*, 2000; Dixon *et al.*, 1988; Zilles *et al.*, 2002). Differences between the feature vectors indicate differences in the shape of the profiles, i.e. in cytoarchitecture. They were measured using the Mahalanobis distance (Mahalanobis *et al.*, 1949; Schleicher *et al.*, 2000). The observer-independent definition of cortical areas is based on the hypothesis that profiles sampled from the same area are similar in shape, resulting in small Mahalanobis distances between their feature vectors. Profiles sampled from different areas differ in shape, resulting in high Mahalanobis distances at their border. To increase the signal-to-noise ratio, distances were calculated between feature vectors from blocks of b ($10 < b < 40$) adjacent profiles, instead of individual profiles. They were analyzed as a function of the profile number of the border between the blocks (Fig. 3*F*). The resulting distance function revealed maxima at those positions where the regions covered by the two blocks showed the most different laminar patterns. The significance of these maxima was evaluated by a Hotelling's T^2-test with Bonferroni-correction for multiple comparisons (Fig. 3*G*). The position of a significant maximum was interpreted as a cortical border, if no higher maximum was found within one block size at either side and the maximum could be reproduced at comparable positions in adjacent sections. These criteria in combination with the use of the Mahalanobis distance function and the applied test for significance allowed to discharge minor variations in cytoarchitecture, corresponding to cortical microcolumns or more gradual cytoarchitectonic changes associated with within-area somatotopy, thus revealing only borders between different cortical areas. Using this approach, four different cytoarchitectonic areas have been identified on the parietal operculum. These areas were well distinguishable from the adjacent insular and parietal cortices as shown in Figure 3*E*. The results of the observer-independent approach were subsequently confirmed by a visual comparison of these quantitative results with the histological sections.

Table 1
Summary of the brains used for cytoarchitectonic analysis of the secondary somatosensory cortex

Case no.	Section no.	Age in years	Gender	Cause of death	Fixative
1	207/84	75	M	Toxic glomerulonephritis	Formalin
2	382/81	59	F	Cardiorespiratory insufficiency	Formalin
3	146/86	37	M	Right heart failure	Formalin
4	71/86	86	F	Cardiorespiratory insufficiency	Formalin
5	68/95	79	F	Cardiorespiratory insufficiency	Bodian
6	2/95	85	F	Mesenteric artery infarction	Bodian
7	16/96	54	M	Myocardial infarction	Formalin
8	2431	39	M	Drowning	Formalin
9	14/94	43	F	Pulmonary embolism	Formalin
10	139/95	74	M	Myocardial infarction	Formalin

Interhemispheric, Interareal and Interindividual Differences

For each brain and area, 50–60 profiles (25–30 per hemisphere) were sampled for further statistical analysis throughout its whole extent (4–10 consecutive sections). Sampled regions were free of histological artifacts and showed a perpendicular orientation of the sectioning plane to the cortical surface. Interhemispheric differences in the shape of the profiles were analyzed using a Monte-Carlo analysis, which tests the differences between the left and right hemispheric profiles against differences between profiles selected randomly from the whole sample. Since this analysis did not show any significant ($P > 0.05$) interhemispheric differences (cf. Fig. 4), profiles of both hemispheres were merged.

Forty mean feature vectors (10 brains, four areas) were calculated, to quantify the individual areal-specific cytoarchitecture. Interareal differences were tested for significance by multivariate one-way repeated measurements analysis of variance (ANOVA; factor: area, blocking factor: subject). The architectonic dissimilarity between the defined areas was visualized by a canonical scatter plot using the first two canonical variables. The degree of dissimilarity between two areas was quantified by the mean Euclidean distance (ED) between their feature vectors (Amunts *et al.*, 2000; Schleicher *et al.*, 2000), which, in contrast to the Mahalanobis distance, quantifies the 'true' distance between the centroids of two multi-dimensional groups without taking into account their variance. The mean ED between corresponding (same) areas of different brains was used to quantify the intersubject variability (high distances indicated a high degree of dissimilarity, i.e. variability). The interindividual differences were subsequently compared with the interareal distances using Student's t-test (Bonferroni-corrected for multiple comparisons).

Results

Four cortical areas were defined by observer-independent cytoarchitectonic mapping, each of which shows a distinct cytoarchitecture. In order to avoid premature speculations about putative functions, we propose a neutral nomenclature for the defined areas. It consists of two parts: OP (for operculum) and a number depending on the caudal to rostral sequence, i.e., OP 1 designates the most caudal area and OP 4 the most rostral.

The Cytoarchitecture of OP 1–OP 4

Area OP 1 (Fig. 5A; cf. Fig. 6)

Layer II of OP 1 was poorly separated from layer III, since its granular cells intermingled with the small pyramidal cells of upper layer III. Layer III showed a subdivision into three

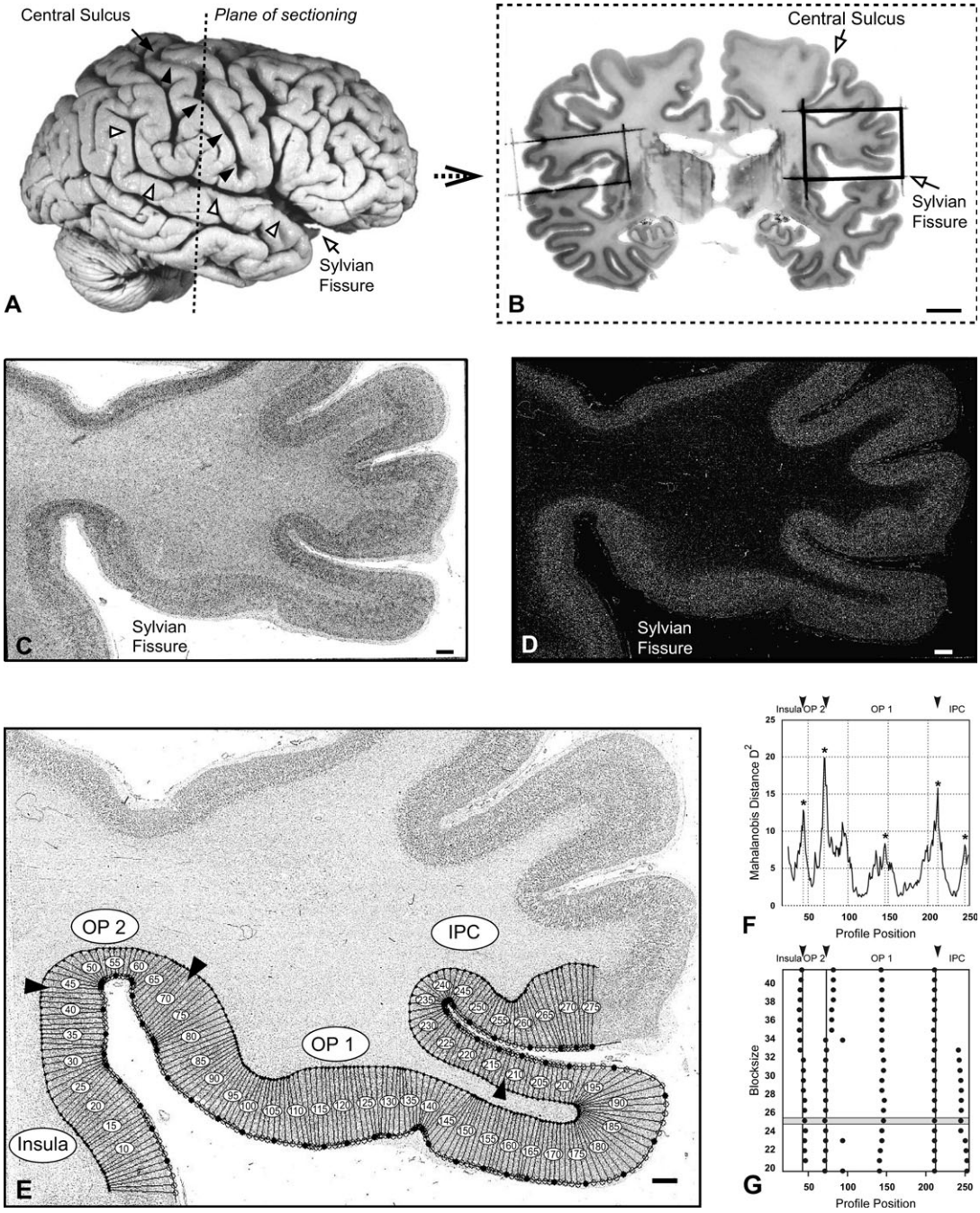

Figure 3. Image acquisition and definition of cortical borders in cell-body-stained histological sections. (*A*) Lateral view on brain 4 after fixation (filled arrowheads mark the central sulcus, empty arrowheads the Sylvian fissure). (*B*) Coronal section number 3586 (cf. dotted line in *A*, left side displayed on the left). Boxes denote the regions of interest (ROI). (*C*) Enlarged view of the right-hemispheric ROI. (*D*) For subsequent cytoarchitectonic analysis the GLI was measured as an index of the volume fraction of cell bodies. Dark pixels correspond to a low volume fraction of cell bodies, light pixels to a high one. (*E*) The cortex was covered by intensity line profiles numbered from 1 to 275. Arrowheads mark the locations of the significant maxima of the distance function as calculated in (*F*). (*F*) Mahalanobis distance function (blocksize $b = 25$) plotted against the profile index. The significant maxima are marked. (*G*) The location of the significant maxima does not depend on the blocksize, but remains stable over large block size intervals. (*B–D*) Bar = 1 mm.

sublayers defined by an increasing size of pyramidal cells. The inner granular layer IV was well separated from the adjacent pyramidal layers (III and V). Layer V contained loosely scattered, medium-sized pyramidal cells. Layer VI contained large cells and appeared slightly more cell-dense than layer V. The cells of layers III–VI were frequently arranged in widely spaced columns reaching into the underlying white matter, which renders the cortex–white matter border less distinct.

The laminar pattern was quantified by the corresponding GLI profile: the GLI peak at the layer II/III border was broad, reflecting the smooth transition between these layers. The numerous large pyramidal cells in deep layer III caused an increase in the GLI curve and separated it from the more cell-sparse middle parts of layer III. The absolute GLI maximum was found in the cell-dense layer IV. The GLI decreased throughout layer V without any detectable sublamination and increased

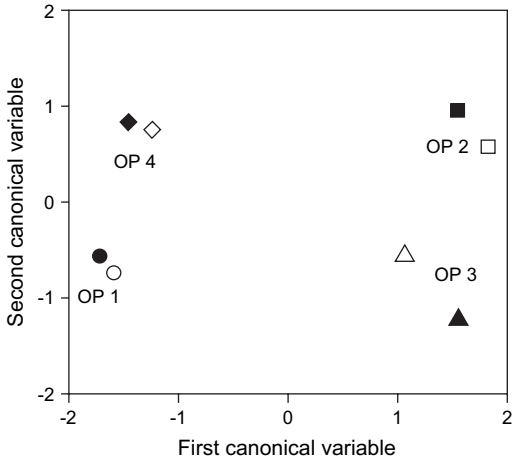

Figure 4. Multidimensional scaling of the inter-areal and inter-hemispheric Euclidean distances. The graph is based on 25–30 sample profiles per area and hemisphere. Filled symbols indicate overall means across all 10 right hemispheres, empty symbols across all 10 left hemispheres. Note, that the inter-hemispheric distances are considerably smaller than the inter-areal distances.

again in layer VI, reflecting its numerous large cells. Finally, a gradual decrease towards the white matter was observed.

Area OP 2 (Fig. 5B*; cf. Figs 6*A *and 8*A*)*

The granular cells of layer II intermingled to such a degree with the small pyramidal cells of layer III, that both layers could not be separated from each other. A pronounced increase in size and density of pyramidal cells throughout layer III as noted in OP 1 was not observed, although a few larger pyramidal cells have been found in deep layer III. The horizontal lamination was more distinct than in OP 1 due to the high cell density in layer IV. Layer V contented mainly small pyramidal cells. Compared with OP 1, OP 2 had thinner infragranular layers and a more sharply defined white matter border.

Since only small pyramidal cells were found in lower layer III, the GLI did not increase at this cortical depth as seen in OP 1. A distinct peak of the GLI profile in layer IV reflected its higher volume fractions of cell bodies as compared with layers III and V. The rapid decrease of the GLI towards the white matter corresponded to the sharp cortex–white matter border.

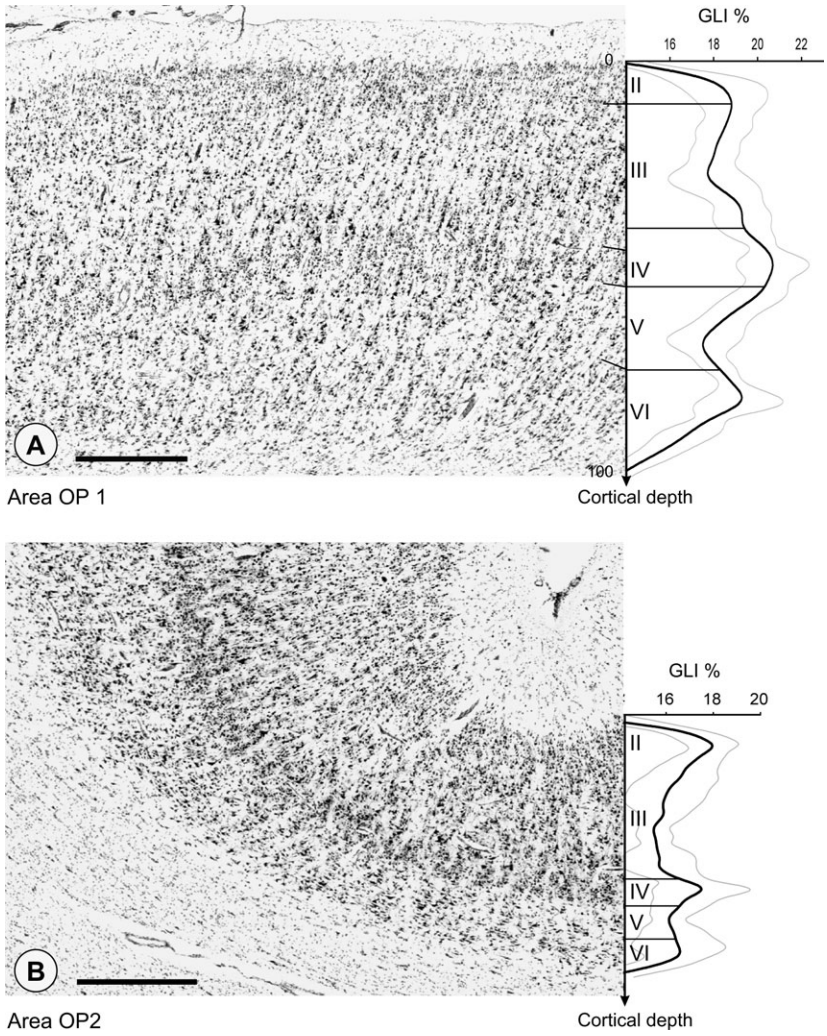

Figure 5. (*A*) Cytoarchitecture of area OP 1 (brain 7, section 4036). OP 1 is characterized by widely spaced cell columns, broad infragranular layers, a blurred cortex-white matter border and large pyramidal cells in sublayer IIIc. Roman numbers designate cortical layers; scale bar = 1 mm. (*B*) Area OP 2, same section. The thin cortex of OP 2 shows small infragranular layers, a sharply defined white matter border and a distinct horizontal lamination. Prominent pyramidal cells in layer III are rare. Roman numbers designate cortical layers; scale bar = 1 mm. The mean (and SD across profiles) of the GLI profiles sampled from exactly the cortex shown in the microphotograph (n = 8–9 profiles) is shown to the right of the images to allow a comparison of the qualitative cytoarchitectonic features and the quantitative representation.

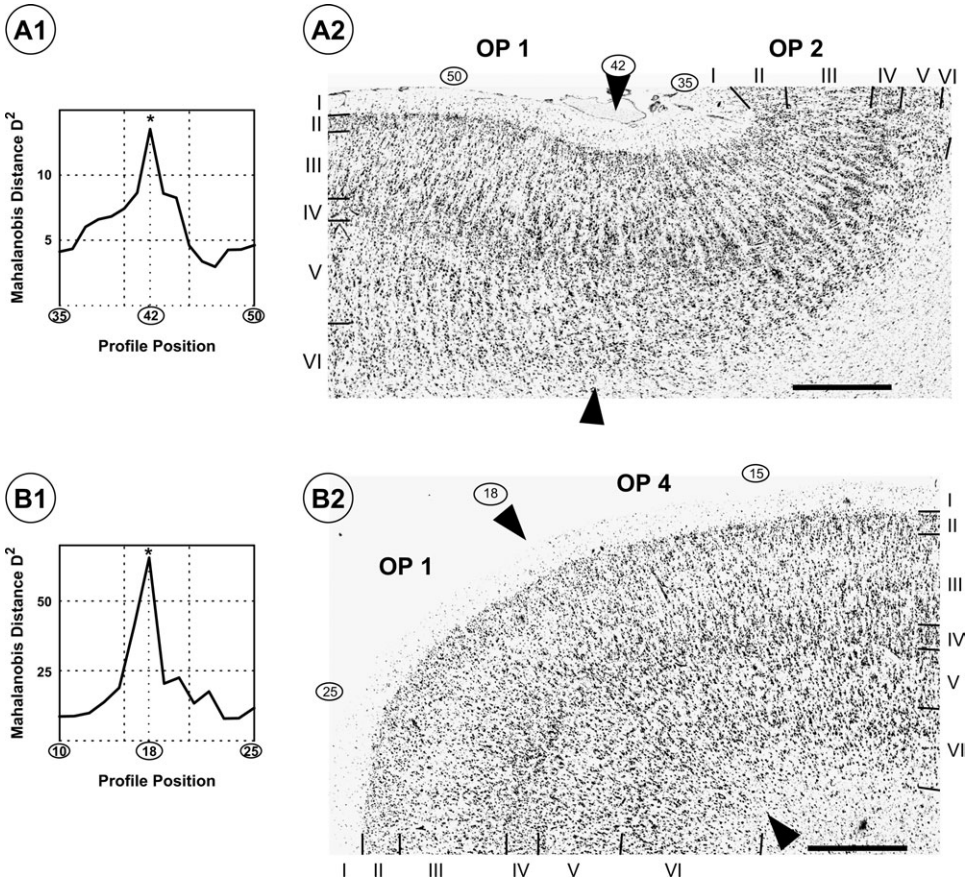

Figure 6. (*A*) Border between OP 1 and OP 2, (brain 7, section 3781). The location of the significant ($P < 0.05$) maximum in the Mahalanobis distance at profile position 42 (*A1*) coincidences with the cytoarchitectonic border (*A2*). Towards OP 2 the horizontal lamination appears more distinct while less and smaller pyramidal cells are found. The blurred white matter border in OP 1 becomes more defined. (*B*) Transition between OP 1 and OP 4 (brain 7, section 4021). The Mahalanobis distance shows a significant ($P < 0.05$) peak at profile position 18 (*B1*). Its position matches the cytoarchitectonic border shown in *B2*. Note the higher volume fraction of cell bodies, the sublamination of layer V, and the less distinct separation of layers III and V from layer IV in OP 4 compared with OP1. Roman numbers designate cortical layers; scale bar = 1 mm.

Area OP 3 (Fig. 7A*; cf. Fig. 8)*

The border of layer II to the cell-sparse layer III was blurred. Layer III showed a low cell packing density and contained only very few large cells. Layer IV and the infragranular layers, which showed a low overall cell packing density, were thin. Layer VI was only slightly more cell-dense than layer V, which contained only very few small pyramidal cells. The white matter border was sharp.

The average GLI was lower than in OP 2 (Fig. 8*A*). The GLI peaks in layer II, IV and VI did not reach such values as in the other opercular areas. In particular, the difference in the GLI between layers V and VI was less pronounced than in OP 4. The distinct border to the white matter was reflected by the sharp decrease in GLI the end of the profile.

Area OP 4 (Fig. 7B*; cf. Figs 6* B *and 8*B*)*

The border between layers II and upper layer III, which contained numerous small pyramidal cells, was inconspicuous. The middle part of layer III was sparse of cells, whereas deep layer III contained many medium-sized pyramidal cells. Layer IV had a moderate cell packing density and was poorly separated from the adjacent pyramidal cell layers. The upper part of layer V contained medium-sized pyramidal cells defining a cell-dense sublayer, which has not been found in any other parietal opercular area. In contrast, the lower sublayer of layer V was rather sparse of cells. The transition between layer VI and the white matter was blurred.

The GLI decreased at the border between layer II and III, which reflected the low packing density of cell bodies in the latter layer. The GLI showed a local minimum in the cell-sparse layer IIIb whereas the numerous large pyramidal cells in IIIc caused an increase in the GLI. The absolute maximum of the GLI profile coincided with the cell-dense layer IV. The subdivision of layer V was reflected by a higher GLI in the cell-dense upper sublayer Va as compared with the more cell-sparse lower sublayer Vb.

Location of OP 1–4 with Respect to Macroanatomical Landmarks

Areas OP 1 (caudally) and OP 4 (rostrally) were located more superficially on the parietal operculum than OP 2 (caudally) and OP 3 (rostrally) (Fig. 9). The border between the superficial and the deep areas was located more medial on the posterior parietal operculum (between OP 1 and OP 2) than on its anterior part (between OP 3 and OP 4). As a consequence, OP 3 had a common border with OP 1 in all hemispheres (section 7 in Fig. 9*A*). OP 1 reached the free surface of the supramarginal gyrus in 16 of the 20 hemispheres, although in five of these hemispheres the dorsal border of OP 1 was located close to the Sylvian fissure. OP 4 was found on the free surface

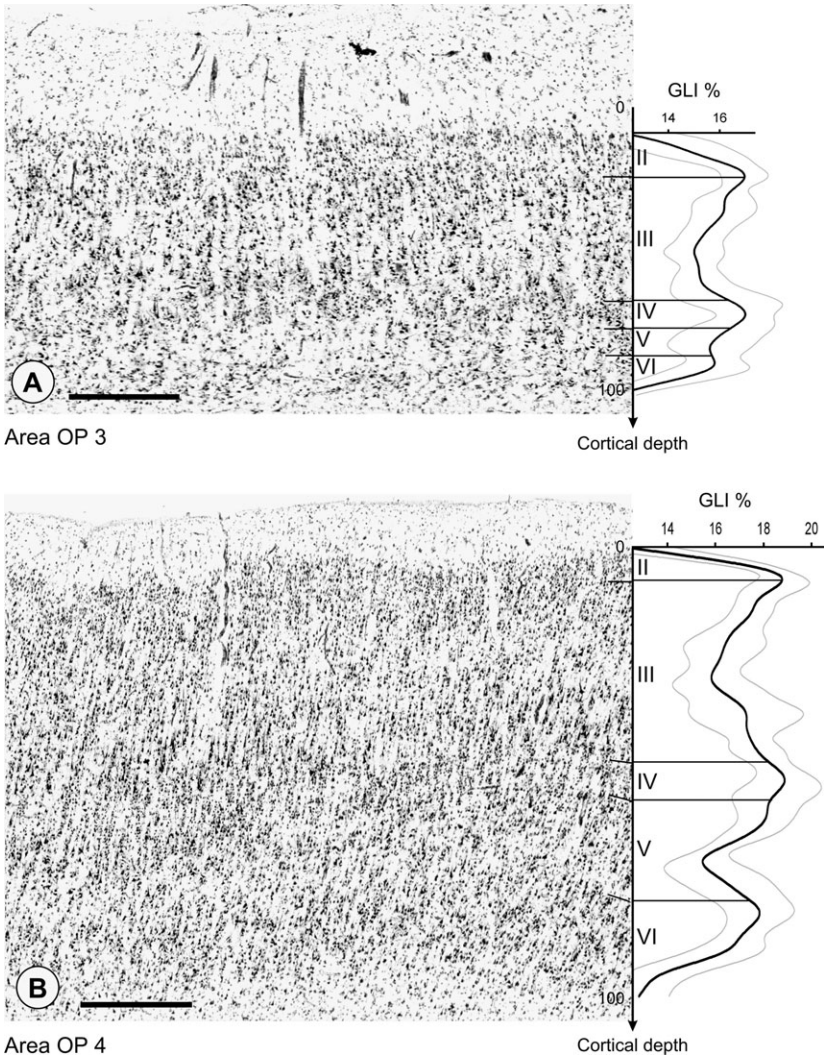

Figure 7. (*A*) Area OP 3, same section as in Figure 5. OP 3 is characterized by a thin cortex and a low overall volume fraction of cell bodies. The subgranular layers are thin and cell-sparse; prominent pyramidal cells are missing. (*B*) Area OP 4, same brain, section 4336. OP 4 shows fine cell columns, large infragranular layers and a blurred transition of layer VI into the white matter. Medium-sized pyramidal cells in lower layer III and upper layer V form a distinct sublamination of these layers. Roman numbers designate cortical layers; scale bar = 1 mm. The mean (and SD across profiles) of the GLI profiles sampled from exactly the cortex shown in the microphotograph (n = 8–9 profiles) is shown to the right of the images to allow a comparison of the qualitative cytoarchitectonic features and the quantitative representation.

(posterior subcentral gyrus) in all hemispheres. Its most dorsal extent was usually (18 of 20 hemispheres) several millimeters apart from the Sylvian fissure. The border between OP 1 and OP 4 was located close to the posterior subcentral sulcus, although both areas could be found on either side of this sulcus. OP 2 and OP 3 were located completely within the Sylvian fissure. Whereas OP 3 sometimes occupied up to three-quarter of the parietal operculum, OP 2 was exclusively located in the depth of the Sylvian fissure. Both OP 2 and OP 3 reached the insular lobe in all 20 hemispheres and cover at maximum its upper third.

OP 4 was the most rostral area in 19 hemispheres. It usually extended approximately to the level of the lateral end of the central sulcus but never reached the precentral part of the subcentral gyrus. This makes the central sulcus a good landmark for the anterior extent of OP 4. OP 1 was the most caudal area in 17 of the 20 hemispheres. OP 1 and OP 2 always extended into the retroinsular region but never reached the caudal end of the Sylvian fissure. Although there was no precise macroscopical landmark for the posterior end these areas, a small gyrus located in the deeper half of the parietal operculum provided a good estimate: In 15 out of the 16 hemispheres where this gyrus was present it was at least partially occupied by OP 1 and/or OP 2 (cf. section 10 in Fig. 9*A*).

Location of OP 1–4 with Respect to Surrounding Cortical Areas

The cytoarchitectonic areas surrounding OP 1–4 are described in clockwise manner (cf. Fig. 9*C*): The cortex located on the precentral (frontal) part of the subcentral gyrus showed clear cytoarchitectonic differences to OP 4. In the anterior subcentral cortex a sublamination of layer V was not found but large pyramidal cells were distributed evenly throughout the whole layer V. The cell density within layer III was considerably lower than in OP 4 (Fig. 10*A*). The extent and possible subparcellations of this region were not examined in this study, since the focus of this examination was on the parietal operculum, whose anterior end is macroscopically defined by level of the central sulcus.

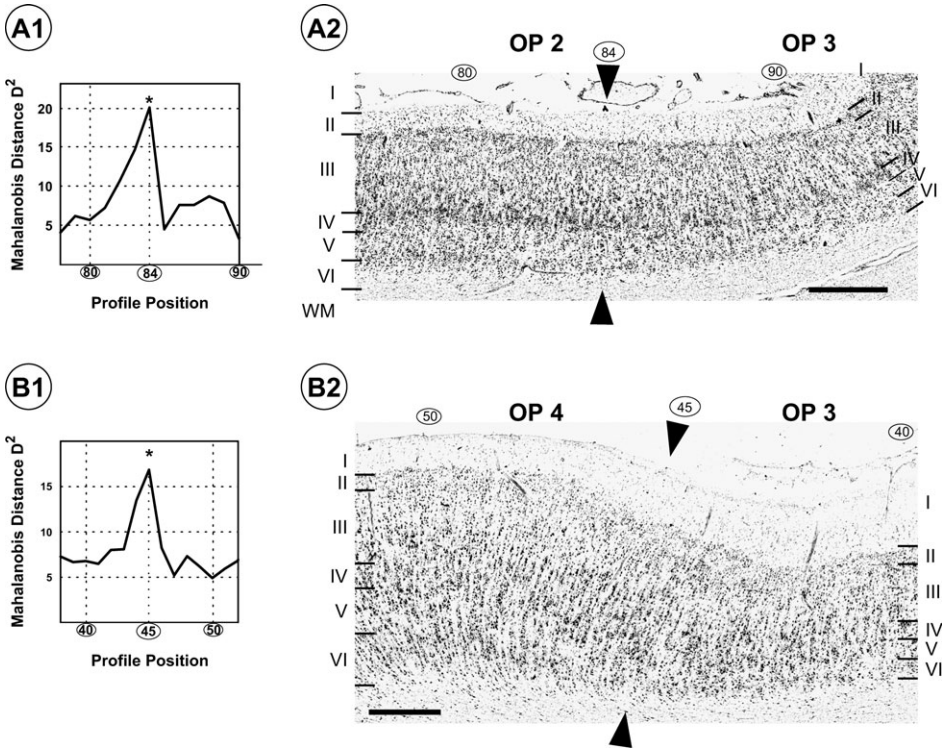

Figure 8. (*A*) Transition from OP 2 to OP 3 (brain 5, section 3946). The border was identified by a significant maximum of the Mahalanobis distance (*A1*) at profile position 84. The corresponding microphotograph is displayed in (*A2*). Note the more perspicuous expression of layers II, IV and VI and the higher overall cell density in OP 2. (*B*) Border between OP 3 and OP 4 (brain 10, section 4041). The location of the significant maximum ($P < 0.05$) of the distance function at profile position 45 (*B1*) matches the change in cytoarchitecture (*B2*). In OP 4, the cortex is thicker and more cell-dense, while the white matter border is less distinct. Prominent pyramidal cells in upper layer V and lower layer III appear area OP 4, forming a distinct sublamination of these layers. Roman numbers designate cortical layers; scale bar = 1 mm.

A common border between OP 4 and the primary somatosensory cortex was observed in 17/20 hemispheres. In detail, area 3a bordered OP 4 in two hemispheres, 3b in 10 hemispheres and BA 2 in seven hemispheres. The most consistent border, which was observed in all 17 hemispheres where OP 4 did neighbor the anterior parietal areas, was the border between OP 4 and area 1. This border was also the most extensive one, whereas the borders between OP 4 and areas 3a, 3b and 2 were usually only observed in very few consecutive sections. Area 1 can be differentiated from OP 4 by its large elongated pyramidal cells in layer lower layer III, its higher cell density and the very pronounced columnar arrangement of its nerve cells (Fig. 10*B*; cf. figures and descriptions in Geyer *et al.*, 1999). The relative thickness of the infragranular layers was smaller in BA 1 than in OP 4. Further caudally OP 1 bordered area 1 in just a single case. A common border between OP 1 and area 2 was only found in the hemisphere where we also observed a border between OP 1 and area 1 and in two additional hemispheres. In all of those hemispheres, OP 4 did also border area 1.

Thus most of the dorsal border of OP 1 was formed by the inferior parietal cortex (IPC), which showed smaller, less prominent pyramidal cells in sublamina IIIc and thinner infragranular layers than OP 1 (Fig. 11*A*).

The cortex caudal to OP 2 was occupied by a retroinsular area (Ri), whose cytoarchitecture was a 'mixture' of features from the IPC and OP 2: the border between OP 2 and the retroinsular cortex was marked by a decrease of cell density in layers IV and VI, a blurring of the white matter border in the retroinsular cortex and appearance of medium sized pyramidal cells in lower layer III, which were not present in OP 2 (Fig. 11*B*). Ventrally OP 2 and OP 3 bordered the granular insular cortex (Ig). This border was characterized by a considerable increase in cortical thickness especially in the subgranular layers and a decrease in the overall cell density. The insular cortex further contained bigger, more prominent pyramidal cells and a less distinct white matter border (Fig. 12).

Interhemispheric, Interareal and Interindividual Cytoarchitectonic Differences

Representative samples of profiles for OP 1–4 were analyzed. No significant cytoarchitectonic differences between the left and right hemispheric samples were found for any area. Thus samples from both hemispheres were merged and 40 mean feature vectors (10 brains, 4 areas) were calculated. The subsequent MANOVA showed that the feature vectors representing areas OP 1–4 differed significantly from each other ($P < 0.05$).

In a next step the average interareal distances representing the differences in cytoarchitecture between OP 1–4 were compared with the interindividual variability of these areas, i.e. the average distance between homologous areas in different brains. The cytoarchitectonic dissimilarities between the different areas (interareal distances) were significantly higher than their interindividual differences for all areas ($P < 0.05$; Fig. 13). Moreover, the interareal distances between OP 1–4 reflected the qualitatively described dissimilarities very well: on visual examination, the most striking cytoarchitectonic differences were found between the superficial areas OP 1 and OP 4 and the

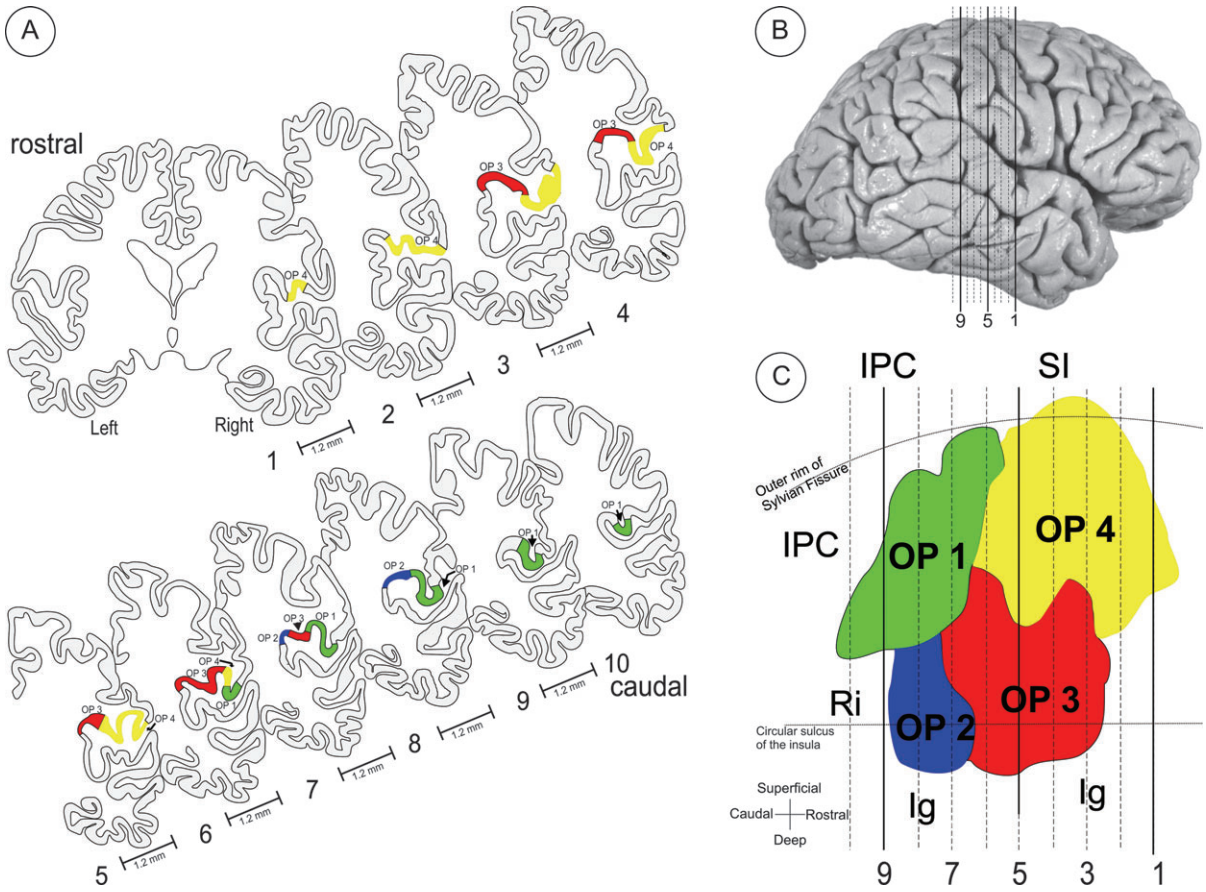

Figure 9. The location of areas OP 1–4 in the right hemisphere of brain 1. (*A*) Drawings of serial coronar sections (right hemisphere displayed on the right side) with OP 1–4 marked by different colors. The section numbers 1–10 correspond to the numbers in (*C*), where the planes of sectioning are marked by lines. (*B*) Brain 1 from right lateral. (*C*) Flat map of OP 1–4 (same brain).

more deeply located OP 2 and OP 3. The corresponding interareal distances were correspondingly high (e.g. ED = 1.39 between OP 1 and OP 2; cf. Fig. 6*A*). The cytoarchitectonic differences were less pronounced between OP 2 and OP 3 or between OP 1 and OP 4 (Fig. 6*B* and 8*A*). This is in good accordance to the lower interareal distances differences between these areas (ED OP 2/OP 3 = 0.75, ED OP 1/OP 4 = 0.56; Fig. 13). Importantly, since this analysis was based on the average laminar patterns of each area as calculated from line profiles sampled across its whole extent these results by no means depend on the location of the different borders relative to the plane of sectioning (which can not be ruled out entirely for the observer-independent mapping algorithm *per se*) but do reflect genuine differences and similarities in cytoarchitecture.

The obtained results were visualized in a canonical scatter plot, where the distances between the symbols reflect the dissimilarity in the shape of the corresponding GLI profiles (Fig. 14). In spite of a considerable interindividual variability, the differences in the profile shapes between the four cortical areas caused the formation of four distinct clusters (OP 1–4). These clusters were separated without any overlap of the 95% confidence areas of each group's centroid.

Discussion

The present study reports four distinct architectonic areas on the human parietal operculum (OP 1–4), which were identified using classical cytoarchitectonic criteria and quantitative cytoarchitectonic analysis. The application of a statistical approach for the detection of areal borders and the quantification of cytoarchitectonic variability in the present study represent an important difference from the classical cytoarchitectonic examinations (e.g. Brodmann, 1909; Sarkissov *et al.*, 1949; von Economo and Koskinas, 1925), which relied purely on visual inspection of histological sections and thus the individual experience of the observer.

With respect to their topography, OP 4 and possibly OP 3 correspond approximately to Brodmann's BA 43. In Brodmann's map, however, BA 43 covers the whole subcentral gyrus (Brodmann, 1909), whereas we described a clearly different cytoarchitecture on the precentral part of this gyrus. BA 40 extends from the intraparietal sulcus to the insular cortex and covers also the parietal operculum. Its border to BA 43 is located approximately at the posterior subcentral sulcus and coincides thus with the location of the border between OP 4 and OP 1. Therefore areas OP 1 (and OP 2) seem to be included among other inferior parietal regions in Brodmann's definition of BA 40.

Later researchers (von Economo and Koskinas, 1925; Sarkissov *et al.*, 1949) found architectonic differences between the inferior parietal cortex and the adjacent operculum (P*F* versus P*F*op; area 40 versus area 40op), which we could confirm by showing significant cytoarchitectonic differences between the IPC and OP 1. Subparcellations within the parietal operculum, however, which may correspond to OP 2 or OP 3, were

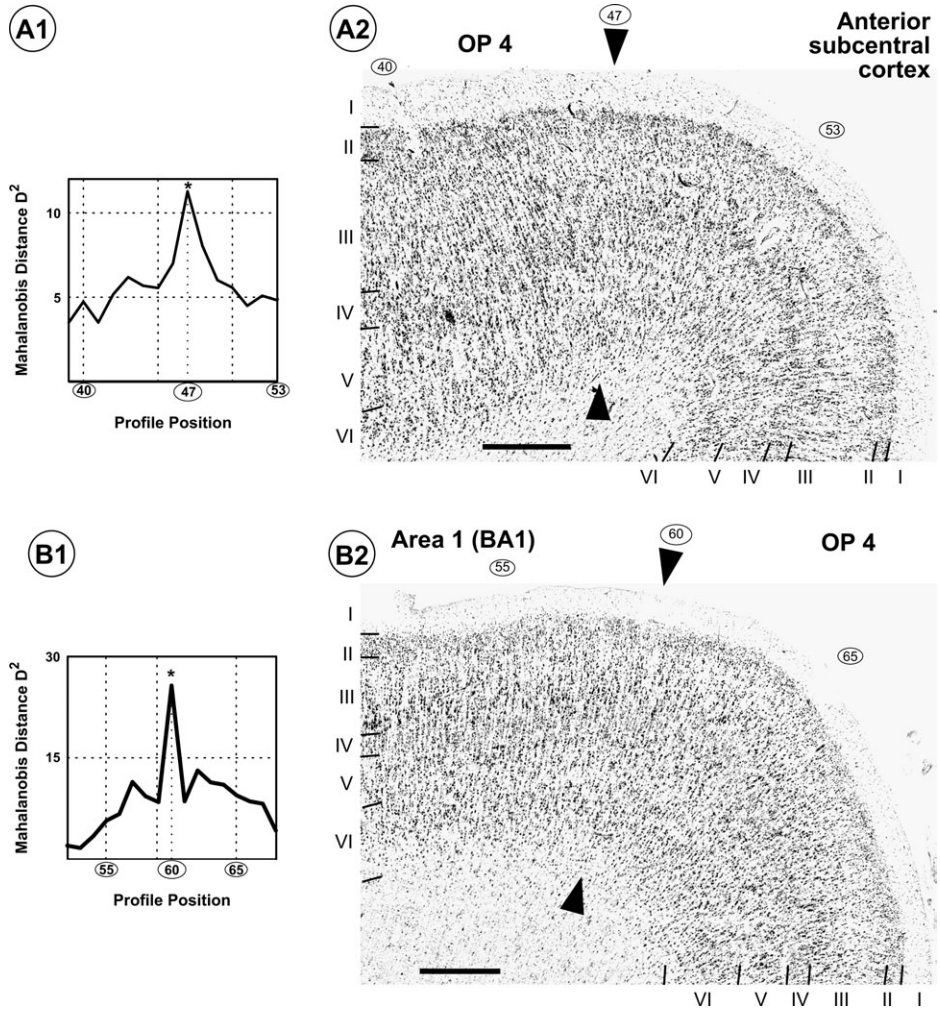

Figure 10. (*A*) Border between OP 4 and the anterior subcentral cortex, i.e. the yet unmapped cortex just anterior to OP 3 and OP 4 on the frontal part of the subcentral gyrus (brain 7, section 4276). The location of the significant ($P < 0.05$) maximum (*A1*) is indicated in the microphotograph (*A2*). Layer V of OP 4 can be subdivided in a more cell-dense Va and a cell-sparse Vb. This sublamination cannot be found in the more anterior subcentral cortex, where pyramidal cells are scattered throughout the whole layer V. The volume fraction of cell bodies of layers III is lower than in OP 4. (*B*) Border between OP 4 and area 1 of the primary somatosensory cortex, (brain 1, section 4186). The location of the significant maximum ($P < 0.05$) of the distance function at profile position 60 (*B1*) matches the change in cytoarchitecture (*B2*). In OP 4, the large and elongated lower layer III pyramids which are characteristic of area 1 (Geyer *et al.*, 1999) discontinue. The overall cell density in OP 4 is lower, the very pronounced columnar arrangement of cells in area 1 is less evident and a subdivision of lamina V into a cell-dense upper and a cell-sparse lower part emerges. Roman numbers designate cortical layers; scale bar = 1 mm.

not described in these maps. Both Sarkissov (1949) and von Economo and Koskinas (1925) defined a separate cytoarchitectonic area on the subcentral gyrus similar in location to OP 4 (areas 43 and PFD respectively). This area was distinguished from the rostrally adjacent agranular motor cortex (due to its well developed layer IV) and the primary somatosensory cortex (e.g., due to smaller cells in deeper layer III). The characterization of PFD provided by von Economo and Koskinas (1925) is close to the description of OP 4: PFD is e.g. described as containing large pyramidal cells in sublayers IIIc and Va. Such cells were also found in OP 4. Like OP 4, PFD has a high cell density, thick infragranular layers and a blurred cortex-white matter border. However, there is one important difference between these maps and our own results. Whereas area OP 4 is followed rostrally by another granular area, PFD and BA 43 border the (agranular) motor cortex. Thus, another cytoarchitectonic entity might be included in the definition of both PFD and BA 43.

Vogt and Vogt (1919) defined several areas on the parietal operculum based on their myeloarchitectonic studies. Two of these areas (areas 73 and 74) are located completely in the depth of the Sylvian fissure. Areas 72 and 88 are located superficially and extend onto the free surface. This myeloarchitectonic parcellation of the parietal operculum is the only 'classical' brain map, which shows multiple cortical areas on the parietal operculum and includes areas, which do not extend onto the free surface. This myeloarchitectonic map is thus most similar to our own cytoarchitectonic results, which also shows the existence of several opercular areas, two of which (OP 2 and OP 3) are not found on the free surface of the brain.

SII Maps in Non-human Primates

The human SII region is considered to be homologous to the SII cortex of non-human primates (Burton *et al.*, 1993; Disbrow *et al.*, 2000). Based on converging evidence from microelectrode mapping, histological examination and tracing experiments on cortico-cortical and thalamic connectivity

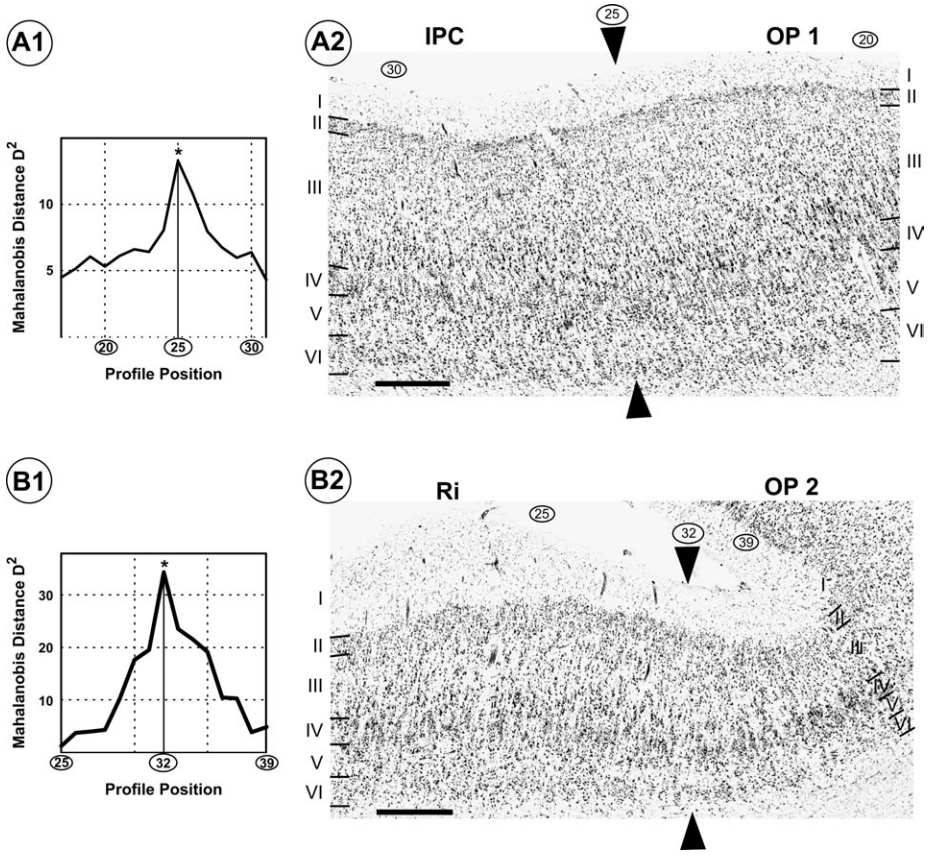

Figure 11. (*A*) Border between OP 1 and the inferior parietal cortex (IPC) (brain 7, section 3661). The position of the profiles and the significant ($P < 0.05$) maximum of the Mahalanobis distance function (*A1*) are indicated in the corresponding cell-body-stained sections (*A2*). In the IPC, the pyramidal cells in layer IIIc are less prominent, layer VI is smaller and forms a more distinct border to white matter. (*B*) Border between OP 2 and the retroinsula (Ri) (brain 7, section 3541). The significant ($P < 0.05$) maximum at position 32 (*B1*), matches the position of cytoarchitectonic changes (*B2*). Towards the retroinsula the cell density in layers IV and VI decreases, medium-sized pyramidal cells in lower layer III appear and the white matter border becomes more blurred. Roman numbers designate cortical layers; scale bar = 1 mm.

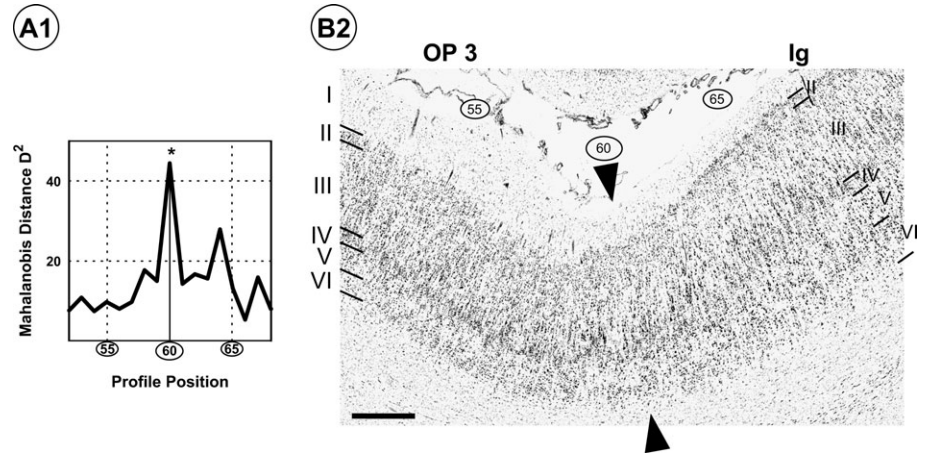

Figure 12. (*A*) Border between OP 3 and the granular insula (Ig) (brain 7, section 4171). The border was identified by the Mahalanobis distance (*A1*), revealing a significant maximum at profile position 60. The location of this profile is marked in the corresponding histological image (*A2*). The insular cortex is thicker, contains bigger, more prominent pyramidal cells and has larger infragranular layers and a more blurred white matter border. Roman numbers designate cortical layers; scale bar = 1 mm.

(Krubitzer *et al.*, 1986, 1993, 1995; Krubitzer and Kaas, 1990; Burton *et al.*, 1995; Disbrow *et al.*, 2003), the existence of multiple areas within the SII region is now considered a general feature of the somatosensory cortex of anthropoid primates (Kaas and Collins, 2003). The most commonly used parcellation scheme for the SII region is as follows (Figs 1 and 15): the opercular area located immediately adjacent to the SI cortex is termed the parietal ventral area (PV). Area PV is followed caudally by area SII. It has to be pointed out, that this 'area SII' is not equivalent to the 'SII region', but denotes an individual area

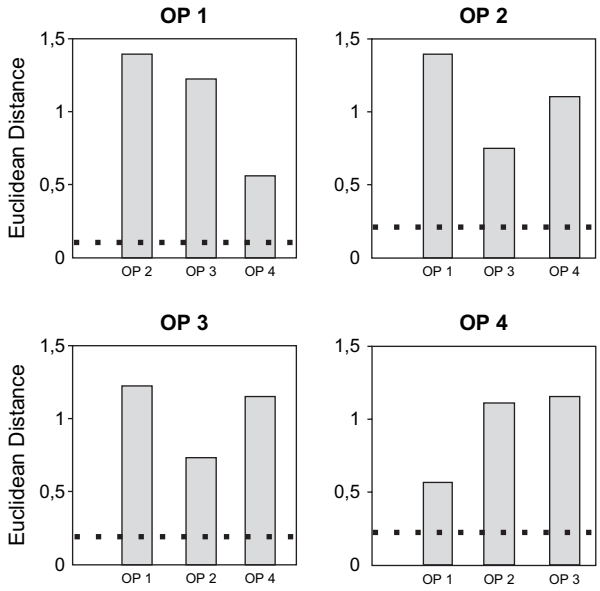

Figure 13. Interindividual variability and interareal cytoarchitectonic differences. The mean Euclidean distance between homologous areas in different brains (i.e. the interindividual variability of OP 1–4) is marked by the dotted lines. The bars denote the mean Euclidean distances between that area and the remaining three (i.e. the dissimilarity between the different areas). Note that the mean distance between different cortical areas is always greater than the interindividual variability across brains.

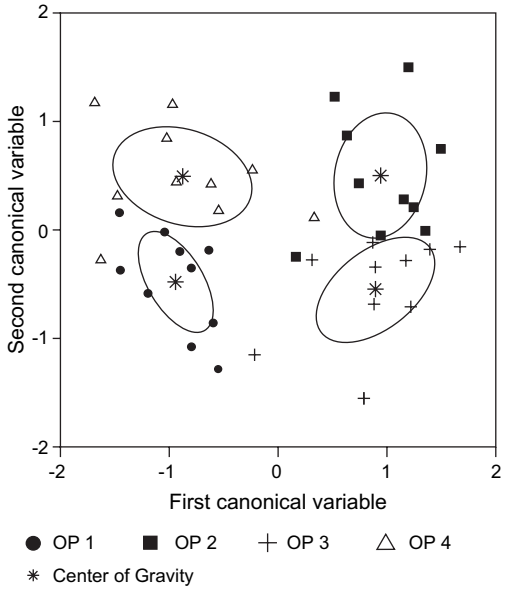

Figure 14. Canonical scatter plot, visualizing the similarities and dissimilarities between mean (50–60 sample profiles) feature vectors from different areas/subjects. Symbols represent the mean feature vector of a single area for an individual brain. Asterisks show the location of the areas' mean feature vectors averaged across all subjects (centroids). The ellipses denote the 95% confidence area of the respective centroids.

within this region. Area VS (ventral somatosensory) is located deeper in the Sylvian fissure medially adjacent to area SII and PV.

Based on its topography OP 4 may correspond to the primate area PV: like PV, OP 4 is located superficially within the Sylvian fissure close to the central sulcus and borders the

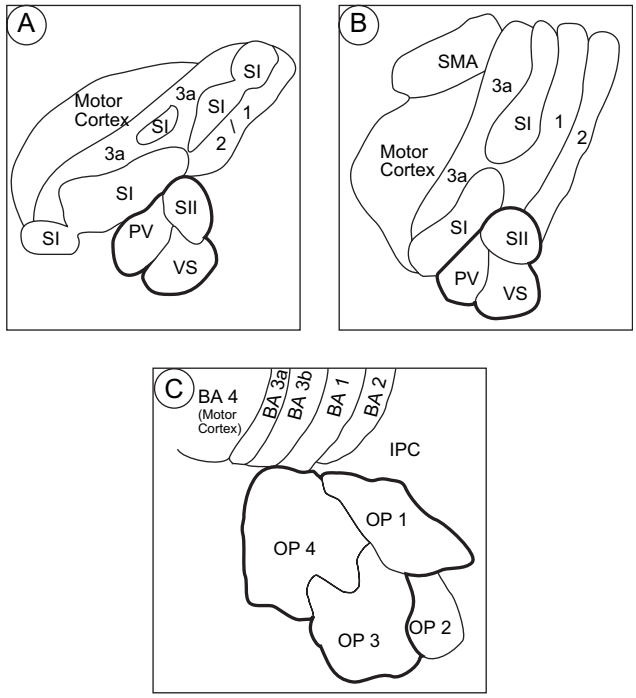

Figure 15. Summary maps of the somatosensory cortex of (*A*) flying foxes (Krubitzer *et al.*, 1993) and (*B*) marmoset monkeys (Krubitzer and Kaas, 1990), both adopted from the author's maps. The maps show a third somatosensory area (VS) within the traditional SII region besides the now well-established areas SII and PV. (*C*) Schematic flatmap of the OP 1–4 on the human parietal operculum and its relation to the surrounding areas (based on brain 1, cf. Fig. 9). Topographically, OP 1 corresponds very well to area SII, whereas OP 4 is located very similar to area PV. This would imply that OP 3 is a human analogue of area VS.

primary somatosensory cortex (SI). OP 1 is located caudally to OP 4 next to the inferior parietal cortex, suggesting that it is a human analogue to area SII. However, the human anatomy seems to differ from the topographical relationships observed for non-human primates in the respect that OP 1 (i.e. area SII) borders the anterior parietal areas 1 and 2 in only a very few cases, whereas in non-human primates there is a consistent border between area SII and area 1 (Coq *et al.*, 2004). Like areas SII and PV, OP 4 and OP 1 share a common border running in a medial to lateral direction. Topologically OP 3 is a good candidate for a human analogue of VS (Fig. 15): OP 3 is located deeper in the Sylvian fissure than OP 1 and OP 4 (which represent the possibly analogue to areas SII and PV) and borders both of these areas. No distinct area has yet been described in SII cortex of non-human primates, which corresponds topographically to OP 2. Most authors examining the cortex posterior to the primate SII region have described the neurons in this region as responding to various and often complex stimuli, including input from other sensory modalities like the auditory and vestibular systems (Robinson and Burton, 1980; Akbarian *et al.*, 1988; Krubitzer *et al.*, 1995; Guldin and Grusser, 1998). In summary, the objectively defined areal boundaries within the human parietal operculum show good agreement with the primate data on that region. This correspondence is be further corroborated by a meta-analysis of human functional imaging studies (Eickhoff *et al.*, 2005), which shows that the functional activations within these areas follow the predictions from primate work: the hand representation within the parietal operculum is found at

the border between OP 1 and OP 4, as is the case for their topographical analogues in the primate brain areas SII and PV.

Functional Inhomogeneity of the Human SII Region

Functional imaging studies on the human somatosensory system provided ample evidence of a functional inhomogeneity of SII. A positron emission tomography (PET) study by Ledberg *et al.* (1995), for example, revealed two separate foci within the parietal operculum. The superficial one was activated by roughness and length discrimination, the deeper one by a somatosensory reaction time task. Two activations within the SII region were also demonstrated in a PET study by Burton *et al.* (1997): an anterior, deep focus was activated as the result of direct touch of the finger, which is mediated mainly by cutaneous receptors. A more caudal, superficial activation was associated with stimulation by a ring like plectrum intended to activate mainly deep receptors. Despite its lower spatial resolution, a magnetoencephalography recording during median nerve stimulation also revealed two consecutive responses located within the SII region. The earlier response was found more anteriorly and medially to the later one (Mima *et al.*, 1997). In an fMRI study, Disbrow *et al.* (2000) stimulated the hand, foot, face, hip and shoulder by sponge brushing. The authors demonstrated two complete, somatotopically organized body maps on the human parietal operculum, probably analogous to the primate areas SII and PV, as well as two additional cortical fields whose somatotopy could not be consistently resolved.

A functional segregation of the human SII cortex was also suggested with respect to pain perception. In a PET experiment, non-painful and painful stimulation resulted in two distinct activation clusters within the SII region (Coghill *et al.*, 1994). A recent fMRI study on the cortical representation of pain and touch confirmed these results by demonstrating two spatially separate activations within SII (Ferretti *et al.*, 2003): one was located on the subcentral gyrus, the other more posterior within the Sylvian fissure. Only the activation of the posterior focus was modulated by the perceived pain intensity. Further evidence that only the posterior parts of the SII region are involved in pain perception was provided by lesion studies: only patients with lesions involving the posterior parietal operculum showed a raised pain threshold on the contralateral body side, whereas patients with more anterior lesions had no deficits in pain perception (Greenspan and Winfield, 1992; Greenspan *et al.*, 1999).

This functional heterogeneity of SII favors the assumption that the four cytoarchitectonic areas on the parietal operculum represent functionally distinct regions. They likely contribute differentially to somatosensory processing tasks (e.g. pain perception, tactile attention and somatosensory working memory) which have been ascribed to SII. If activities from all four areas have been labeled as located within 'SII', this might potentially have caused confusion about the function of the SII region. To answer the question of the functional meaning of the structural differentiation, it is now necessary to correlate the defined cytoarchitectonic areas with functional imaging data as shown in Eickhoff *et al.* (2005).

Notes

This Human Brain Project/Neuroinformatics research was funded jointly by the National Institute of Mental Health, of Neurological Disorders and Stroke, of Drug Abuse, the National Cancer Center, the Deutsche Forschungsgemeinschaft (KFO-112) and the Volkswagenstiftung.

Address correspondence to Professor Karl Zilles, Institut für Medizin, Forschungszentrum Jülich GmbH, D-52425 Jülich, Germany. Email: K.Zilles@fz-juelich.de.

References

Akbarian S, Berndl K, Grusser OJ, Guldin W, Pause M, Schreiter U. (1988) Responses of single neurons in the parietoinsular vestibular cortex of primates. Ann N Y Acad Sci 545:187–202.

Adrian ED (1940) Double representation of the feet in the sensory cortex of the cat. J Physiol 98:16–18.

Amunts K, Malikovic A, Mohlberg H, Schormann T, Zilles K (2000) Brodmann's areas 17 and 18 brought into stereotaxic space — where and how variable? Neuroimage 11:66–84.

Annett M (1973) Handedness in families. Ann Hum Genet 37:93–105.

Aziz Q, Schnitzler A, Enck P (2000) Functional neuroimaging of visceral sensation. J Clin Neurophysiol 17:604–612.

Brodmann K (1909) Vergleichende Lokalisationslehre der Großhirnrinde. Leipzig: Barth.

Burton H (1986) Second somatosensory cortex and related areas. In Cerebral cortex, sensory-motor areas and aspects of cortical connectivity (Jones EG, ed.), pp. 31–98. New York: Plenum.

Burton H, Sinclair RJ (2000) Attending to and remembering tactile stimuli: a review of brain imaging data and single-neuron responses. J Clin Neurophysiol 17:575–591.

Burton H, Videen TO, Raichle ME (1993) Tactile-vibration-activated foci in insular and parietal–opercular cortex studied with positron emission tomography: mapping the second somatosensory area in humans. Somatosens Motor Res 10:297–308.

Burton H, Fabri M, Alloway K (1995) Cortical areas within the lateral sulcus connected to cutaneous representations in areas 3b and 1: a revised interpretation of the second somatosensory area in macaque monkeys. J Comp Neurol 355:539–562.

Burton H, MacLeod AM, Videen TO, Raichle ME (1997) Multiple foci in parietal and frontal cortex activated by rubbing embossed grating patterns across fingerpads: a positron emission tomography study in humans. Cereb Cortex 7:3–17.

Coghill RC, Talbot JD, Evans AC, Meyer E, Gjedde A, Bushnell MC, Duncan GH (1994) Distributed processing of pain and vibration by the human brain. J Neurosci 14:4095–4108.

Coq JO, Qi H, Collins CE, Kaas JH (2004) Anatomical and functional organization of somatosensory areas of the lateral fissure of the New World titi monkey (*Callicebus moloch*). J Comp Neurol 476:363–387.

Disbrow E, Roberts T, Krubitzer L (2000) Somatotopic organization of cortical fields in the lateral sulcus of *Homo sapiens*: evidence for SII and PV. J Comp Neurol 418:1–21.

Disbrow E, Litinas E, Recanzone GH, Padberg J, Krubitzer L (2003) Cortical connections of the second somatosensory area and the parietal ventral area in macaque monkeys. J Comp Neurol 462:382–399.

Dixon WJ, Brown MB, Engelman L, Hill MA, Jennrich RI (1988) BMDP statistical software manual. Berkeley, CA: University of California Press.

Eickhoff S, Amunts K, Mohlberg H, Zilles K (2005) The human parietal operculum. II. Stereotaxic maps and correlation with functional imaging results. Cereb Cortex doi:10.1093/cercor/bhi106.

Ferretti A, Babiloni C, Gratta CD, Caulo M, Tartaro A, Bonomo L, Rossini PM, Romani GL (2003) Functional topography of the secondary somatosensory cortex for nonpainful and painful stimuli: an fMRI study. Neuroimage 20:1625–1638.

Geyer S, Schleicher A, Zilles K (1999) Areas 3a, 3b, and 1 of human primary somatosensory cortex: 1. Microstructural organization and interindividual variability. Neuroimage 10:63–83.

Greenspan JD, Winfield JA (1992) Reversible pain and tactile deficits associated with a cerebral tumor compressing the posterior insula and parietal operculum. Pain 50:29–39.

Greenspan JD, Lee RR, Lenz FA (1999) Pain sensitivity alterations as a function of lesion location in the parasylvian cortex. Pain 81:273–282.
Guldin WO, Grusser OJ (1998) Is there a vestibular cortex? Trends Neurosci 21:254–259.
Kaas JH, Collins CE (2003) The organization of somatosensory cortex in anthropoid primates. Adv Neurol 93:57–67.
Krubitzer LA, Kaas JH (1990) The organization and connections of somatosensory cortex in marmosets. J Neurosci 10:952–974.
Krubitzer LA, Sesma MA, Kaas JH (1986) Microelectrode maps, myeloarchitecture, and cortical connections of three somatotopically organized representations of the body surface in the parietal cortex of squirrels. J Comp Neurol 250:403–430.
Krubitzer LA, Calford MB, Schmid LM (1993) Connections of somatosensory cortex in megachiropteran bats: the evolution of cortical fields in mammals. J Comp Neurol 327:473–506.
Krubitzer L, Clarey J, Tweedale R, Elston G, Calford M (1995) A redefinition of somatosensory areas in the lateral sulcus of macaque monkeys. J Neurosci 15:3821–3839.
Lam K, Kakigi R, Mukai T, Yamasaki H (2001) Attention and visual interference stimulation affect somatosensory processing: a magnetoencephalographic study. Neuroscience 104:689–703.
Ledberg A, O'Sullivan BT, Kinomura S, Roland PE (1995) Somatosensory activations of the parietal operculum of man. A PET study. Eur J Neurosci 7:1934–1941.
Lotze M, Wietek B, Birbaumer N, Ehrhardt J, Grodd W, Enck P (2001) Cerebral activation during anal and rectal stimulation. Neuroimage 14:1027–1034.
Mahalanobis PC, Majumda DN, Rao DC (1949) Anthropometric survey of the united provinces. A statistical study. Sankhya 9:89–324.
Merker B (1983) Silver staining of cell bodies by means of physical development. J Neurosci Methods 9:235–241.
Mima T, Ikeda A, Nagamine T, Yazawa S, Kunieda T, Mikuni N, Taki W, Kimura J, Shibasaki H (1997) Human second somatosensory area: subdural and magnetoencephalographic recording of somatosensory evoked responses. J Neurol Neurosurg Psychiatry 63:501–505.
Penfield W, Jasper H (1954). Epilepsy and functional anatomy of the human brain. Boston, MA: Little, Brown & Co .
Peyron R, Garcia-Larrea L, Gregoire MC, Costes N, Convers P, Lavenne F, Mauguiere F, Michel D, Laurent B (1999) Haemodynamic brain responses to acute pain in humans: sensory and attentional networks. Brain 122:1765–1780.
Robinson CJ, Burton H (1980) Somatic submodality distribution within the second somatosensory (SII), 7b, retroinsular, postauditory, and granular insular cortical areas of M. fascicularis. J Comp Neurol 192:93–108.
Sarkisov SA, Filimonoff IN, Preobrashenskaya NS (1949) Cytoarchitecture of the human cortex cerebri. Moscow: Medgiz.
Schleicher A, Zilles K (1990) A quantitative approach to cytoarchitectonics: analysis of structural inhomogeneities in nervous tissue using an image analyser. J Microsc 157:367–381.
Schleicher A, Amunts K, Geyer S, Kowalski T, Schormann T, Palomero-Gallagher N, Zilles K (2000) A stereological approach to human cortical architecture: identification and delineation of cortical areas. J Chem Neuroanat 20:31–47.
Vogt C, Vogt O (1919) Allgemeinere Ergebnisse unserer Hirnforschung. Journal für Psychologie und Neurologie 25:279–461.
von Economo K, Koskinas G (1925) Die Cytoarchitektonik der Hirnrinde des erwachsenen Menschen. Wien: Springer.
Woolsey CN, Erickson TC, Gilson WE (1979) Localization in somatic sensory and motor areas of human cerebral cortex as determined by direct recording of evoked potentials and electrical stimulation. J Neurosurg 51:476–506.
Wree A, Schleicher A, Zilles K (1982) Estimation of volume fractions in nervous tissue with an image analyzer. J Neurosci Methods 6:29–43.
Xu X, Fukuyama H, Yazawa S, Mima T, Hanakawa T, Magata Y, Kanda M, Fujiwara N, Shindo K, Nagamine T, Shibasaki H (1997) Functional localization of pain perception in the human brain studied by PET. Neuroreport 8:555–559.
Zilles K (2004) Architecture of the human cerebral cortex. Regional and laminar organization. In: The human nervous system (Paxinos G, ed.), pp. 997–1055. San Diego, CA: Elsevier.
Zilles K, Armstrong E, Schleicher A, Kretschmann HJ (1988) The human pattern of gyrification in the cerebral cortex. Anat Embryol (Berl) 179:173–179.
Zilles K, Schleicher A, Palomero-Gallagher N, Amunts K (2002) Quantitative analysis of cyto- and receptor architecture of the human brain. In: Brain mapping, the methods (Mazziotta J, Toga A, eds), pp. 573–602. San Diego, CA: Academic Press.